Modeling of hydrophilic wafer bonding by molecular dynamics simulations

David A. Litton and Stephen H. Garofalini[a)]
Department of Ceramic and Materials Engineering, Interfacial Molecular Science Lab, Rutgers University, 607 Taylor Road, Piscataway, New Jersey 08854-8065

(Received 31 July 2000; accepted for publication 31 December 2000)

The role of moisture in hydrophilic wafer bonding was modeled using molecular dynamics computer simulations of interface formation between amorphous silica surfaces. Three different surface treatments were used in order to determine the effect of moisture on the formation of siloxane (Si–O–Si) bridges across the interface at two temperatures. The three surface conditions that were studied were: (a) *wet* interfaces containing 1 monolayer of water adsorbed at the interface (based on the room temperature bulk density of water), (b) *hydroxylated* interfaces with concentrations of 3–5 silanols/nm^2 on each surface and no excess water molecules initially in the system, and (c) *pristine* interfaces that had only Si and O and no water or H present. The surfaces were slowly brought together and siloxane bond formation was monitored. In the pristine interfaces, siloxane bridges formed across the interface by the coalescence of various defect species in each surface. A bimodal distribution of siloxane bond angles formed during the first 2.5 Å of approach after the first siloxane bond was formed. These bond angles were much lower than and higher than the bulk average, indicating the formation of less stable bonds. The hydroxylated (with no excess water) and wet surfaces showed a more uniform distribution of siloxane bond angles, with no highly reactive small bond angles forming. The presence of water molecules enhanced H-bond formation across the interface, but trapped water molecules inhibited formation of the strong siloxane bridges across the interface. In real systems, high temperatures are required to remove this trapped moisture.
 [DOI: 10.1063/1.1351538]

I. INTRODUCTION

Wafer bonding technology takes advantage of the ability to develop strong adhesion between mirror-polished surfaces at room temperature without the use of glues or high pressures[1–5] and an excellent review of wafer bonding is available.[6] Interfaces and junctions can thus be created between high quality bulk wafers with low dislocation densities and little contamination. Costly ion implantation or deep diffusion processes can also be avoided. This technique is used in the processing of silicon-on-insulator devices, micromechanical systems, and power devices.[1–5] Although the bulk of the research in this area has been focused on silicon wafers, with and without surface layers of silicon dioxide, recent efforts to bond a variety of materials have been reported.[7] Wafer-scale integration of numerous materials as well as potential three-dimensional (3D) integration affords great flexibility in integrated circuit design and miniaturization.

The necessary surface flatness for successful wafer bonding is characterized on two size regimes. State-of-the-art polishing techniques result in peak-to-valley height deviations on the order of 1 μm over lateral dimensions also on the order of 1 μm. If the microroughness of the polished surfaces is sufficiently low, micron-scale waviness can be tolerated since the materials can elastically deform to accommodate the mismatch.[8] Root-mean-square (rms) microroughness on the order of 0.5 nm is sufficient to achieve room temperature wafer bonding between clean surfaces.[5,6]

The presence of dust particles on the wafer surfaces must be avoided to achieve complete bonding. Dust particles on the order of microns result in unbonded regions on the order of millimeters.[1] In general, wafer bonding is done in a cleanroom environment, although forcing de-ionized (DI) water between the surfaces as they are contacted has been shown to obviate the need for a dust-free environment.[9]

In addition to mirror polishing and avoidance of dust particles, wet chemical treatments are necessary for strong room temperature bonds. For silicon wafer bonding, treatments have been optimized to produce either hydrophilic or hydrophobic silicon surfaces.[1,5,10] Hydrophilic surfaces are generated by immersing wafers in basic, oxidizing solutions usually containing hydrogen peroxide or ammonium hydroxide. This removes adsorbed impurities and produces surface layers of SiO_2 with thicknesses on the order of a few nanometers. After this treatment, wafers are rinsed with DI water and spin dried. Several investigators have carefully characterized the surfaces resulting from these preparatory steps using a variety of analytical techniques.[11–15] They found that the SiO_2 surfaces are terminated with silanol ($\equiv$Si–OH) groups and a 3D network of chemisorbed and physisorbed water molecules. Investigators have reported rms microroughnesses ranging from 1 to 5 Å for these surfaces. Room temperature bond energies on the order of 0.2 J/m^2 for bonded hydrophilic wafers are reported in several studies.[1,3,5,8,14–16] Hydrogen bonds between silanols and wa-

[a)]Author to whom correspondence should be addressed; electronic mail: shg@glass.rutgers.edu

ter molecules are believed to be the source of these bond energies.[5,7,14]

Tong and Goesele have developed a detailed model to describe the experimental data obtained in studies of room temperature bonding and subsequent annealing of hydrophilic wafers.[6] They propose that for room temperature bonding, chains consisting of three or more hydrogen-bonded water molecule bridge the interface. This is based on the fact that hydrogen-bonded water triplets are more stable than single water molecules or dimers, and the observation that strong wafer bonds require surfaces with rms microroughness less than 0.5 nm. Water triplets could then bridge the mean 1 nm gap between surfaces. They also point out that two main types of silanols are present on SiO_2 surfaces: singular silanols ($\equiv$Si–OH) and associated silanols ($\equiv$Si–OH–O–Si$\equiv$), the latter commonly called vicinal silanols. However, there is a third important type of silanol not discussed by them called the geminal silanol ($=$Si–$(OH)_2$). The geminal silanol site has two OHs on a single Si, and geminals make up ~20%–25% of the silanols on silica surfaces.[17] Geminal sites may therefore be an important component in hydrogen bonding between surfaces. Based on the hydrogen bond energies and IR and HREELS reports of their concentrations, theoretical wafer bond energies of 0.165 J/m^2 were calculated.[6] This compares well with the experimental ''saturated'' value of 0.24 J/m^2 for stored wafers bonded at room temperature.

Experiments have shown that bond energies of wafer pairs aged for hundreds of hours at room temperature increase by more than a factor of 2.[7,10,12] However, initial bond energies immediately after bonding are usually only ~0.05–0.06 J/m^2, rising to the higher, saturated value of 0.24 J/m^2 after days of storage or elevated temperature annealing.[6] Furthermore, chemical shifts in XPS and HREELS[11] experiments indicate that the mean siloxane (Si–O–Si) bond angle of the 1 nm oxide layers (~130°) prepared by wet chemical means is less than the value for bulk SiO_2(~144 °C). This indicates that the oxide is strained due to the Si/SiO_2 interface. Experiments[18–20] and computer simulations[21–23] have shown that water molecules preferentially attack low-angle siloxane bonds by a hydrolytic decomposition reaction:

$$H_2O + \equiv Si–O–Si\equiv \rightarrow \equiv SiOH + \equiv SiOH. \quad (1)$$

The saturated wafer bond energies were observed to increase exponentially with annealing temperature between 110 and 150 °C. Since experiments had shown that water desorbs from silica surfaces at any relative humidity above 110 °C,[24–26] it can be assumed that water molecules diffuse away from the interface and siloxane bonds form across the interface by the condensation of adjacent silanols on opposite surfaces. The condensation reaction is the reverse of Eq. (1). Wafer bond energies near 1.5 J/m^2 were found to be nearly constant between 150 and 800 °C,[6] which can be attributed to complete condensation of all silanols that were adjacent across the interface to siloxane bonds. The density of siloxane bonds across the interface was assumed to be lower relative to bulk SiO_2 due to microroughness resulting in incomplete contact. Accordingly, the saturated wafer bond energies were lower than bulk SiO_2.

Molecular dynamics (MD) computer simulations of interface formation between SiO_2 surfaces have shown the importance of separation distance on siloxane (Si–O–Si) bond formation,[27] which is relevant to surfaces that have subnanometer roughness. These simulations also showed the effect of temperature on the change from a surface diffusion mechanism to a viscous flow mechanism. Below ~1100 °C, surface diffusion from an ~5 Å asperity dominated, while temperatures >1100 °C, mechanisms involving exchange between atoms in a surface asperity with atoms in the subsurface occurred.[27] Simulations also showed the effect of slight compression of silica surfaces on surface structure[28,29] and the enhanced reactivity of such surfaces after subsequent exposure to moisture.[23,30] MD simulations of interfaces of silica surfaces with several monolayers of water molecules between them have also been studied[31] using the multibody potentials previously presented[21,27,30,32] and used in the work presented below. In the Timpel *et al.* study, siloxane bond formation across the interface as a function of temperature was studied. Interface siloxane bonding increased with increasing temperature. The directional dependence of the diffusion of water molecules and dissociated water species in the interface region was analyzed. At low temperatures, diffusion of water species was limited to translation along the interface. Near T_g, significant diffusion of O^{2-} and H^+ ions into the bulk of the glasses was observed.

However, as discussed above, the experimentally observed increase in saturated wafer bond energies as temperature is increased to ~110–150 °C, remaining constant up to 800–900 °C, indicates the importance of water removal on siloxane bond formation across the interface. There is, however, a question regarding how much water is present at the interface during various stages in annealing. The previous simulations showed the anisotropy of water migration as a function of temperature.[31] Thus, water may remain in certain portions of the interface, trapped by structural or energetic impediments. In the current study, we apply molecular dynamics computer simulations to determine the necessary conditions and mechanisms to form siloxane bonds across silica interfaces at temperatures well below the glass transition temperature as a function of water concentration at the interface. The interfaces were formed under conditions of constant volume and energy (microcanonical ensemble) by advancing the top surface into the bottom surface by 0.1 Å every 2 ps. This allowed sufficient time for atoms to equilibrate as the interfaces were formed at the lower temperatures used in this study.

Three types of model interfaces were investigated in this study. Hydroxylated silica surfaces with approximately 1 monolayer of excess water between them were brought together to model wafers with water trapped between the surfaces. These interfaces will be referred to as ''wet'' interfaces. Hydroxylated surfaces with concentrations of 3–5 silanols/nm^2 and no excess water molecules were also brought together to model interfaces in which water had been removed. These will be called ''hydroxylated'' interfaces. Finally, pure silica fracture surfaces that had never been reacted with water were brought together to remove the effects of silanols and water molecules on siloxane bonding across

TABLE I. Parameters in the two-body term of the potential.

Atom pair	$A_{ij}(\times 10^{-8}$ ergs)	β_{ij} (Å)	ρ_{ij} (Å)
Si–Si	0.187 70	2.29	0.29
Si–O	0.296 20	2.34	0.29
Si–H	0.006 90	2.31	0.29
O–O	0.072 50	2.34	0.29
O–H	0.039 84	2.26	0.29
H–H	0.003 40	2.10	0.35

TABLE II. Parameters for V^{CSF}.

Atom pair	$a(\times 10^{-12}$ ergs)	b(Å^{-1})	c(Å)
Si–H	−4.6542	6.0	2.20
H–H	−5.2793	6.0	1.51
	+0.3473	2.0	2.42
O–H	−2.0840	15.0	1.05
	+7.6412	3.2	1.50
	−0.8336	5.0	2.00

the interface. These will be called ''pristine'' interfaces. Each system was brought together at room temperature and at a higher temperature sufficient to desorb water from the surfaces, but well below the T_g of the model glass. Thus we isolate the role of temperature on interface siloxane bridge formation over a temperature range similar to that reported in experiments.

II. COMPUTATIONAL PROCEDURE

The MD technique was used to simulate the formation of silica–silica interfaces. A multibody potential function was used to describe the interactions between ions in this study. The overall potential function is the sum of a modified Born–Mayer–Huggins (BMH) pair potential V_{ij}^{BMH} and a three-body potential V_{jik}. The modified BMH pair potential is the sum of a short-range repulsive term and a modified Coulombic term

$$V_{ij}^{(2)}=A_{ij}\exp\left(\frac{-r_{ij}}{\rho_{ij}}\right)+\frac{q_iq_j}{r_{ij}}\xi\left(\frac{r_{ij}}{\beta_{ij}}\right)+V_{ij}^{CSF}, \tag{2}$$

where $r_{ij}=|\mathbf{r}_i-\mathbf{r}_j|$, q_i=the formal ionic charge on atom i, and A_{ij}, ρ_{ij}, and β_{ij} are adjustable pair parameters. ξ is the complimentary error function used to reduce the formal charges (q_iq_j) as a function of separation distance, thus creating a screened Coulomb potential. In the form of the potential used here, the β_{ij} is dependent on the $i-j$ pair, which offers significant flexibility in altering the product of the charges.[33]

V_{ij}^{CSF} is used to add additional structure to the potential and is given as

$$V_{ij}^{CSF}=\sum_{x=1}^{6}\frac{a_{ij}^{(x)}}{1+\exp(b_{ij}^{(x)}(r_{ij}-C_{ij}^{(x)}))}. \tag{3}$$

V_{ij}^{CSF} is zero for most pair interactions presented below, but is useful in simulations involving H interactions.[32] The parameters used in the repulsive and screened Coulomb terms are listed in Table I, while those in V_{ij}^{CSF} are listed in Table II.

The three-body potential function was included to account for the directional nature of the bonding in silica and water. It acts as a penalty function, which raises the energy of the system when the angles between covalently bonded species deviate from the preferred angle. This potential was applied to all Si–O–Si, O–Si–O, Si–O–H, and H–O–H first neighbor triplets as defined by the following formulas:

$$V_{jik}^{(3)}=\left\{\lambda_{jik}\exp\left[\frac{\gamma_{ij}}{r_{ij}-r_{ij}^0}+\frac{\gamma_{ik}}{r_{ik}-r_{ik}^0}\right]\Omega_{jik}\right\}, \tag{4}$$

when $r_{ij}<r_{ij}^0$ and $r_{ik}<r_{ik}^0$,

$V_{ijk}^{(3)}=0$ otherwise.

Ω_{jik}, the angular term, is a function of θ_{jik}, the angle formed by atoms j, i, and k with atom i at the vertex. The three-body term is a penalty function that increases the potential (and repulsive forces) whenever a three atom triplet deviates from an ideal angle. The parameters used for the three-body interactions are listed in Table III.

When calculating the potential energy and net force on a given atom, all atoms within a sphere of radius 5.5 Å were considered. The trajectories of atoms were determined by solving Newton's classical equations of motion using a fifth-order Nordsieck–Gear predictor–corrector algorithm. The simulations were performed in the microcanonical ensemble, under conditions of constant number, volume, and energy. A 0.1 fs time step was used in systems containing hydrogen ions. The time step used in simulations of pristine silica systems was 1.0 fs.

This multibody potential and MD technique has been used successfully to simulate several materials. Static structure factors and radial distribution functions of simulated bulk silica (SiO_2) glass match well with experimental data.[34] Four common crystalline polymorphs, α- and β-quartz and α- and β-cristobalite are stable with this potential, with a change in lattice parameters of 1%–5% from experimental data for quartz and 4%–5% for cristobalite. (Note that there was a typo in the original paper[34] in that the heading of the β terms in Table I were mixed (β_{Si-Si} should have been in the β_{Si-O} location, β_{Si-O} should have been in the β_{O-O} location, and β_{O-O} should have been in the β_{Si-Si} location). Using the

TABLE III. Parameters in the three-body term.

	O–Si–O	Si–O–Si	Si–O–H	H–O–H
$\lambda(\times 10^{-11}$ ergs)	19.0	0.3	5.0	35.0
γ (Å)				
Si–O	2.8			
O–Si		2.0	2.0	
O–H			1.2	1.3
r^0(Å)				
Si–O	3.0			
O–Si		2.6	2.6	
O–H			1.5	1.6
θ^c(deg)	109.5	109.5	109.5	104.5

mislabeled parameters would give very high pressures for the glass and much larger deviations of the crystals from the experimental data.

Defect species concentrations and hydroxylation of silica surfaces were also consistent with experiment.[21,22,35] The polymerization of silicic acid to form a silica gel was simulated, producing good agreement with experimental data for activation energies of polymerization and the relative time evolution of Si Q_n species.[32,36,37] The surface structure and energies of simulated crystalline Al_2O_3 (Ref. 38) were similar to previous simulations[39] as well as more recent *ab initio* calculations.[40] More complex layered oxides V_2O_5 and γ-LiV_2O_5 were also simulated using these potentials, with structural and vibrational data similar to experiment, as well as the appropriate phase transition to δ-LiV_2O_5 as Li ions entered the V_2O_5 crystal.[41]

Interface systems with three different surface treatments were analyzed in this study, as mentioned above. *Pristine* interfaces were formed between two simulated annealed surfaces of vitreous silica. *Hydroxylated* interfaces were generated by reacting these pristine surfaces with water, then removing unreacted water molecules such that stoichiometry was maintained. Water molecules were not removed in the *wet* interfaces. Two different surfaces were made by heating stoichiometric mixtures of atoms to 10 000 K for 20 ps to form a low viscosity liquid. Glasses were formed by quenching these liquids stepwise to 300 K via 10 ps runs through intermediate temperatures of 8000, 6000, 4000, 3000, 2000, 1000, and 300 K. In each of these simulation steps, constant temperature was maintained for the first 2 ps to allow the systems to equilibrate, in addition to the constant number and volume conditions. Thereafter, constant energy conditions were imposed. Periodic boundary conditions were applied in the *x, y,* and *z* directions to simulate effectively infinite bulk glasses. Each glass consisted of 2400 ions with dimensions 3.57 by 3.57 by 2.85 nm.

Fracture surfaces were created on both bulk glasses by immobilizing 600 atoms at the bottom of the simulation cells and removing the periodic boundary conditions in the *z* direction. Thus the ions at the top of the simulation cell are in direct contact with a vacuum above them. To allow the surfaces to relax, 10 ps simulations were run at 2000, 1000, and 300 K.

To create wet surfaces, 64 water molecules were randomly placed above each relaxed surface over 40 ps intervals at 2000 K. This number of water molecules was chosen such that approximately 1/2 monolayer would be present on each surface. This calculation was done assuming a monolayer thickness of 3 Å over the 12.8 nm^2 surface area of the simulation cell, and assuming a density of 1 g/cm^3. Reflecting boundaries were placed 5 Å above the positions of the original *z* periodic boundaries in the bulk silica systems in order to prevent loss of the water molecules at elevated temperature and 150 ps simulations were run at 2000 K. The wet surfaces were then cooled to room temperature through 10 ps simulations at 1500, 1000, and 300 K.

Hydroxylated surfaces were generated by removing any oxygen or hydrogen ions that were neither network species, nor bonded to network species. Oxygen ions within 2.0 Å of any silicon ion were considered network species. Hydrogen ions within 1.2 Å of any network oxygen ions were considered bonded to those ions. Stoichiometry was maintained adding hydrogen or oxygen ions to reasonable sites on the surface to restore the proper ratios. The hydroxylated surfaces were then relaxed again with 10 ps runs at 2000, 1500, 1000, and 300 K, again with reflecting boundaries.

To create interfaces, one surface of each type (pristine, hydroxylated, or wet) was inverted onto the other surface of the same type. The initial volume of each of these three interfaces was set such that the smallest distance between any two ions on different surfaces was 6.0 Å. Thus, in the initial configurations, there were no interactions across the interface, since an interaction cutoff of 5.5 Å was used in these simulations. Periodic boundary conditions were applied in the *x, y,* and *z* directions. However, since a frozen layer more than 6 Å thick was present at both the bottom of the simulation cell and at the top of the simulation cell (since the top of the cell consisted of an inverted surface system), no interactions nor transport occurred across the *z* boundaries in the interface simulations.

In summary, the initial configuration of the pristine silica interface consisted of 1600 Si and 3200 O ions in a simulation cell with *x, y,* and *z* dimensions of $3.57\times3.57\times6.36$ nm, respectively. The original hydroxylated interface system consisted of 1600 Si, 3254 O, and 108 H ions with *x, y,* and *z* dimensions of $3.57\times3.57\times6.72$ nm, respectively. The top surface in this interface had a hydroxyl coverage of 5.3 OH^-/nm^2, while that of the bottom surface was 3.1 OH^-/nm^2. The initial wet interface configuration consisted of 1600 Si, 3328 O, and 256 H ions with cell *x, y* and *z* dimensions of $3.57\times3.57\times7.19$ nm, respectively. Although results for one interface of each type will be discussed herein for the sake of clarity, several samples of each system type were analyzed, with little variation in results observed.

Interfaces were formed from these initial configurations by advancing the top surface toward the bottom surface. This advancement was accomplished by reducing the *z* coordinate of all network Si and O ions in the top surfaces. Hydrogen ions and O ions in water molecules were not considered as a part of the top surface during this movement since their mobility precluded permanent assignment to either surface. For the pristine and hydroxylated interfaces, the first angstrom of the approaches was done by advancing the top surface 0.5 Å after every 2 ps simulation run. These large advances were justified since very few pairs of atoms were within the interaction cutoff distance at these interface separations. Thereafter, the top surfaces were advanced 0.1 Å after every 2 ps simulation run. Temperature was held constant for the first 0.4 ps of each simulation run. In the wet interface systems, due to the presence of mobile water molecules that interacted across the interface, the 0.1 Å step was used throughout the approach. The rate of approach is well below the sound velocity and allows sufficient time for water molecules to interact with the surface. The top surfaces were advanced into the bottom surfaces until significant siloxane bonding was observed in all interface types, as will be discussed in Sec. III.

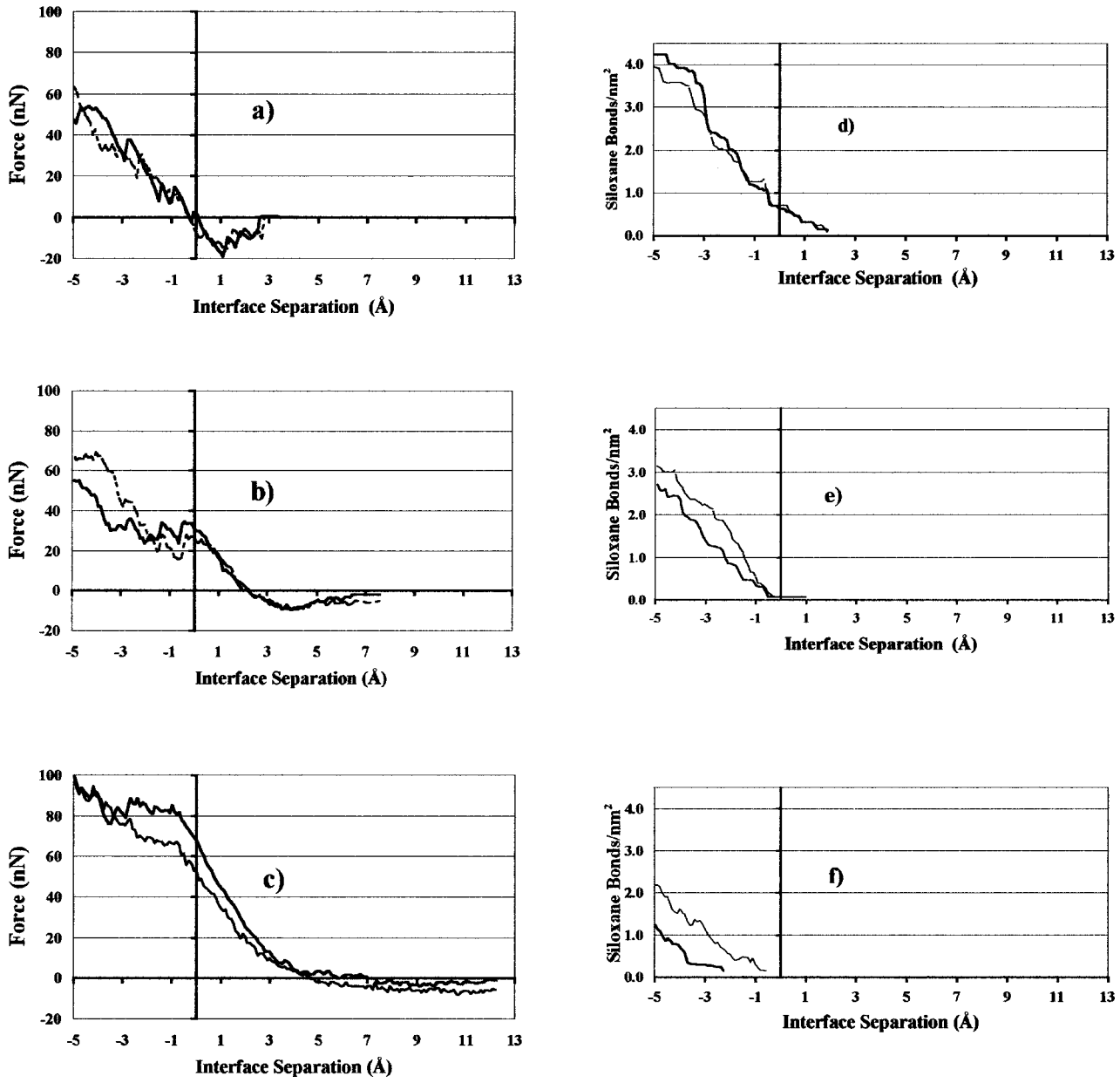

FIG. 1. (a)–(c) The z component of the force on the top surfaces as a function of interface separation for both temperatures of the: (a) pristine, (b) hydroxylated, and (c) wet interface systems. (d)–(f) Plots of the number of siloxane bridges across the interface normalized to the area of the interface as functions of interface separation; (d) pristine, (e) hydroxylated, (f) wet. Heavy solid line at 300 K, lighter dashed line at 1000 K for each part.

During the approach runs, the average net z component of the force on the network Si and O ions in the top surface from interactions with all other ions in the system (within the interaction cutoff) was calculated as a function of separation distance. Again, O ions in water molecules and all H ions were not included as atoms in the top surface in this calculation since they could not be permanently assigned to either surface. These forces did not include the first 0.4 ps of each simulation, during which time the temperature was held constant.

In addition to the net z component of force, the angles of any Si–O–Si (siloxane) bonds that formed across the interfaces were calculated and recorded every 10 fs. A bond across the interfaces was considered to exist when any O ion in the system was within 2.0 Å of any two Si ions on opposite surfaces. The coordination environment surrounding any ion participating in a siloxane bridge across the interface was also recorded every 10 fs.

III. RESULTS AND DISCUSSION

The net z component of the force on the network atoms comprising the top surface was calculated in order to compare the interactions between the various surfaces as they were brought together to form interfaces at two temperatures. The numbers of siloxane bonds (..Si–O–Si..) across the interface were also determined during the approach. The force and siloxane bond data for each interface type studied are shown as functions of interface separation distance in Figs. 1(a)–1(f). In Figs. 1(a)–1(c), positive values of force indi-

cate net repulsion, while negative values indicate net attraction. The volume of the simulation cells of all systems was the same for a given interface separation value in Figs. 1(a)–1(f). The zero point of interface separation was arbitrarily chosen as the point where the net *z* component of the force on the top surface of the lower temperature pristine system became repulsive (>0) after passing through a minimum (which corresponds to the maximum attraction). This is consistent with conventions used in atomic force microscopy studies.

The net *z* component of the force on the top surface was calculated every 100 fs and averaged over the 2 ps intervals between each movement of the top surface to generate the curves in Figs. 1(a)–1(c). In the pristine systems [Fig. 1(a)], the approach of the top surface toward the bottom surface was started at a distance such that atoms on opposite surfaces were noninteracting (beyond the cutoff distance). Thus, the net *z* component of the force was initially zero. Net repulsive force was observed for the initial cross–interface interactions, although it was of such small magnitude that the repulsion was not observable on the scale used in Fig. 1(a). This repulsion is consistent with the outward relaxation of oxygen atoms on the silica surfaces reported in previous simulations and experiments.[35,42–44] Such relaxation would lead to oxygen–oxygen repulsion as the initial cross–interface interaction. At slightly less than 3 Å separation, the net *z* components of force became attractive (<0). Maximum attraction was observed at approximately 1 Å separation for both temperatures. As shown in Fig. 1(d), the first siloxane bonds across the interface formed at approximately 2 Å separation for both temperatures. Thus the attractive regimes of the force–distance curves [Fig. 1(a)] coincide with the formation of siloxane bonds across the interface.

The hydroxylated interfaces were also formed at an initial separation distance chosen such that atoms on opposite surfaces were noninteracting, although the presence of the hydroxyls on the surfaces enables a net attraction caused by hydrogen bonding, as shown in Fig. 1(b). Maximum attraction was observed at approximately 4 Å separation for both temperatures, and the net *z* components of force became repulsive at approximately 2 Å separation. One siloxane bond formed across the lower temperature interface at 1 Å separation, as shown in Fig. 1(e). A monotonic increase in the number of bonds across this interface was observed starting at −0.5 Å. This was also the separation distance at which siloxane bonding across the higher temperature interface was first observed. The net *z* component of force on the top surfaces was repulsive when siloxane bonding began across the hydroxylated interfaces [Fig. 1(b)].

With regard to hydrogen bonding across the interface, Fig. 2 shows the numbers of SiO–H–OSi bonds across the hydrated and wet interfaces as a function of interface separation. Any H atoms within 1.8 Å of two O atoms that were within 2.0 Å of Si atoms on opposite surfaces were considered to be members of SiO–H–OSi bonds. Thus both hydrogen bonds (O–H bond lengths 1.2–1.8 Å) and silanol bonds (OH bond lengths <1.2 Å) were counted. These bonds will hereafter be referred to as single hydroxyl bridges. Interface separations were determined exactly as in Fig. 1. Curves

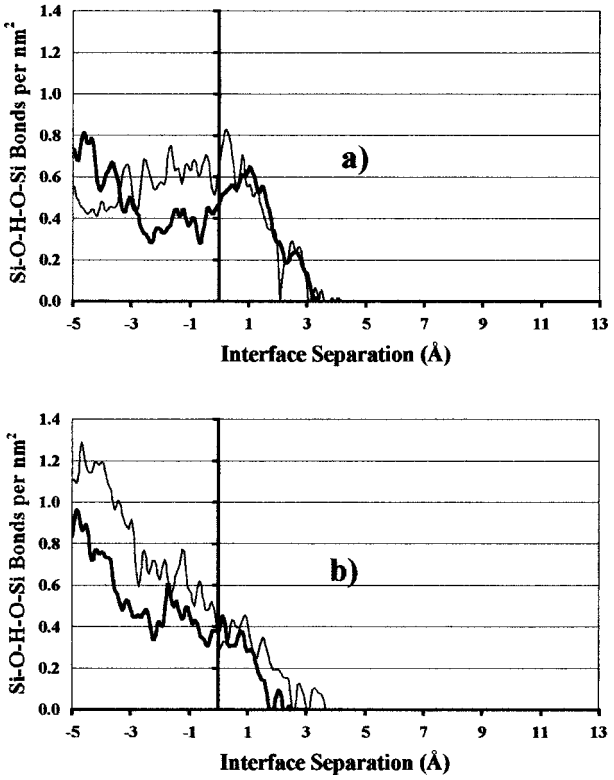

FIG. 2. The number of single hydroxyl bridges across the interface normalized to the interface area as a function of interface separation at both temperatures for: (a) hydroxylated and (b) wet interface systems. Heavy solid line at 300 K, lighter line at 1000 K.

were drawn for both temperatures studied. Data for the hydroxylated and wet systems are presented in Figs. 2(a) and 2(b), respectively. In the hydroxylated systems [Fig. 2(a)], formation of these hydroxyl bridges began at approximately 3 Å separation, in the attractive regime of the force–distance curve in Fig. 1(b). The fact that these systems reached maximum net attraction before single hydroxyl bridges formed can be understood in terms of increased hydrogen bonding between oxygen atoms on the top surface and hydrogen atoms adsorbed on the top surface.

The wet interface systems were also started at a separation distance chosen such that atoms on both surfaces were noninteracting, but net attraction was initially observed [Fig. 1(c)] since interactions with water molecules adsorbed to the top surface were included in the calculations of net force on this surface. In comparison to Figs. 1(a) and 1(b), Fig. 1(c) shows that there is a longer range attraction in the system with more water molecules caused by the H_2O present in the gap between the surfaces. However, the presence of water molecules between the surfaces subsequently inhibits formation of siloxane bonds across the interface [Fig. 1(f)].

Single hydroxyl bridges in the wet systems formed at interface separations similar to those in the hydroxylated interfaces (~2–3.5 Å), as can be seen by comparing Fig. 2(b) to Fig. 2(a). Siloxane bonding in the higher temperature wet system initiated at the same interface separation (~−0.5 Å) as in the hydroxylated systems [Figs. 1(e) and 1(f)]. However, the lower temperature wet system was advanced an additional 1.5 Å before siloxane bonds began to form [Fig.

1(f)]. Because of periodic boundaries perpendicular to the surface (in x and y), the concentration of water molecules between the surfaces was constant. Since the experimental diffusion constant of water at moderate bonding temperatures is too low to enable water to diffuse from the central area of a bonded wafer to exit at the edge, the simulation is relevant to locations between bonded wafers where small areas of water molecules are trapped or unable to diffuse away from the interface. Although limited diffusion of water molecules into the glasses was observed at both temperatures, many water molecules remained in the interface region throughout the approach simulations. These trapped water molecules delayed siloxane bonding relative to the hydroxylated systems at the lower temperature, but not at the higher temperature. The diffusion of water ~10 Å into the subsurface followed a low density path or channel caused by the ring-like structure of silica. Such channels have been observed in previous simulations of silica.[45,46]

After initial siloxane bond formation across the interface in the pristine system, application of compressive stress leads to further bonding across the pristine interfaces at both temperatures, as can be seen by comparing Figs. 1(a) and 1(d). Very similar forces and bonding behavior were observed at both temperatures studied.

The first siloxane bridge across the interface in the hydroxylated system at 300 K formed at approximately 1 Å separation [Fig. 1(e)]. A monotonic increase in the number of siloxane bridges was observed below −0.5 Å separation. This separation also corresponded to the initiation of siloxane bridging in the higher temperature system. Thus applied stresses of approximately 2–3 GPa were required to initiate significant siloxane bonding in the hydroxylated interface systems [Fig. 1(b)]. It should be noted that the internal pressure of bulk silica simulated at constant volume using these potentials is ~2–3 GPa (but can be readily lowered to near atmospheric pressure by only slightly reducing the long range tail of the O–O potential). Thus, compression up to this pressure is only overcoming this artificial bulk-like repulsion.

As shown in Figs. 1(e) and 1(f), more siloxane bonds formed across the interface as a function of interface separation at the higher temperatures as compared to the lower temperatures. This may be a result of the effect of different silicon Q_n species (where, using the NMR nomenclature, n equals the number of bridging oxygen on the Si, such that Si atoms bonded to one NBO and three BO are called Q_3 species, and so on). While most silanol (SiOH) sites on the surface are Q_3 species, about 20%–25% are Q_2 species.[17] These Q_2 species are commonly called geminal silanols (2 hydroxyls on a single Si). Their formation would enhance bonding across the interface because of the increased lability of a Q_2 with only 2 siloxane bonds attaching this Si to the glass surface versus 3 such bonds in a Q_3.

Temperature had a strong effect on the bonding across the interface in the wet systems. Both hydroxyl bridges and siloxane bridges formed earlier in the approach at the higher temperature [Figs. 2(b) and 1(f)]. More hydroxyl bridges were present in the higher temperature system throughout the approach [Fig. 2(b)]. The net z component of force on the top surface was lower as a function of interface separation at the higher temperature [Fig. 1(c)].

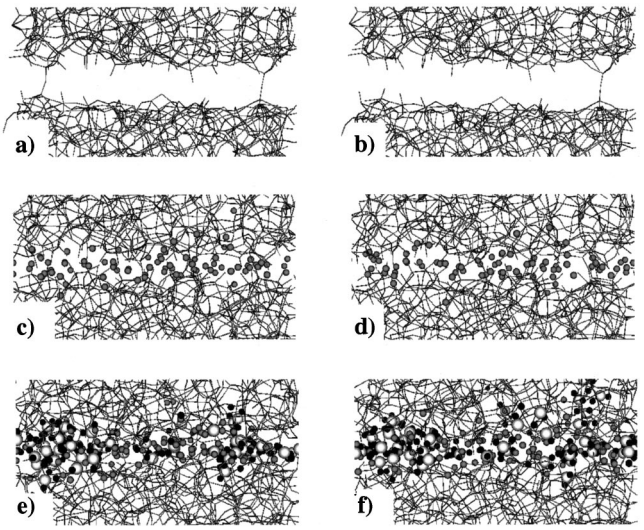

FIG. 3. Snapshots of the interfaces at the initiation of siloxane bridging across the interface at 300 K (a), (c), (e) and 1000 K (b), (d), (f). Si–O bonds are drawn lines. Small, light spheres represent H atoms bonded to network oxygen atoms. Small, dark spheres represent H atoms bonded to oxygen atoms in water molecules. Large spheres represent O atoms in water molecules: (a)–(b) pristine; (c)–(d) hydroxylated; (e)–(f) wet. Note penetration of H and water into the silica in (c)–(f).

At the higher temperature, water molecules were more mobile and could dissociate more easily as compared to that at the lower temperature. The higher mobility allowed water molecules to rearrange under applied stress, thus reducing the observed stress on the higher temperature system and forming more hydroxyl bridges.

Figure 3 shows snapshots of simulation graphics taken at the end of the 2 ps interval of the approach during which siloxane bonding across the interface began for each system studied. Figure 3(a) shows the lower temperature pristine interface at a separation of 2 Å. Bonds are drawn between each Si and O atom within 2.0 Å of each other in this figure—no atoms are drawn. Two bonds across the interface are evident. Figure 3(b) shows the initiation of bonding in the higher temperature pristine system, which occurs at the same interface separation. No significant difference was observed in the interface structure at the higher temperature, though one less bond had formed at this point in the approach.

As apparent in the smaller gap between the surfaces in Figs. 3(c) and 3(d), the top surfaces must be moved significantly closer to the bottom surfaces to initiate siloxane bonding in the hydroxylated systems. The interface separation in these figures was −0.5 Å, corresponding to the initiation of significant siloxane bonding in the lower and higher temperature systems, respectively. The figure also shows that at this nominal separation distance of −0.5Å, there is still no significant overlap between the two surfaces. The spheres drawn represent hydrogen atoms that are bonded to network oxygen atoms. However, only Si–O bonds are drawn. Two siloxane bonds across the interface are present in both systems.

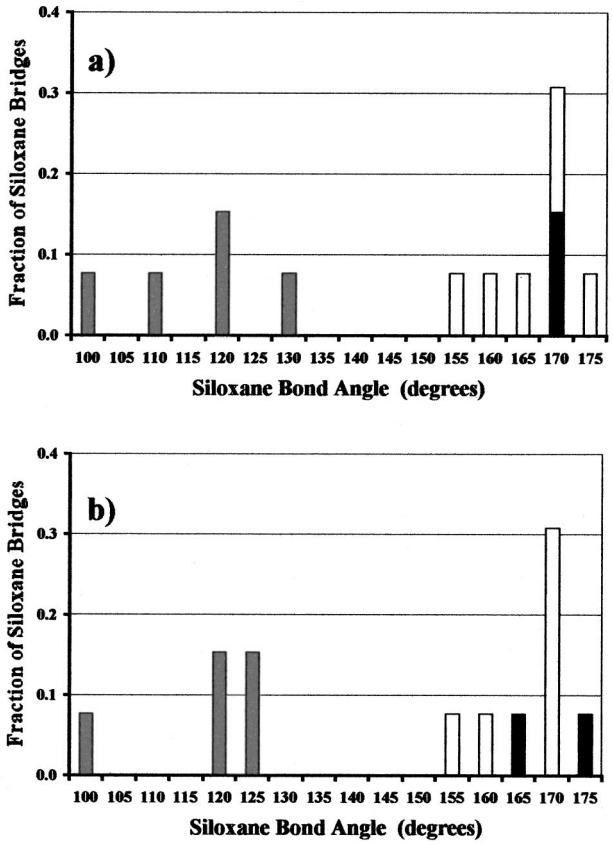

FIG. 4. The fraction of siloxane bridges that form across the pristine interfaces with the initial siloxane bond angles within the indicated ranges at (a) 300 K and (b) 1000 K. The black shading of the bar indicates a nonbridging oxygen bonds to an SiO_3; the gray shading indicates OSi_3 formation; the white bar indicates formation via an SN_2 mechanism. Data are from bonds that form after the surfaces move 2.5 Å closer than the distance of the first siloxane bond formation.

Snapshots of the wet interface systems at the onset of siloxane bridging are shown in Figs. 3(e) and 3(f). The smaller, lighter shaded spheres again represent H atoms bonded to network O atoms. The darker small spheres represent H atoms bonded to O atoms that are not bonded to the network, and are thus members of water molecules, OH^- or H_3O^+ complexes. These O atoms are indicated as the larger, light shaded spheres in Figs. 3(e) and 3(f). Clearly water molecules are trapped at the interface. However, diffusion into the network is apparent in the upper right side of Fig. 3(e) and especially 3(f). Again, only Si–O bonds are drawn, and two siloxane bridges are present in each system. Not drawn in the figure is the significant amount of H bonding that occurs across the interface.

The simulation results are in qualitative agreement with the model of Tong *et al.*[6,7] They attribute the initial room temperature bond energy of hydrophilic wafer pairs to hydrogen bonds. We observe that without the application of stress, hydroxylated and wet silica interfaces are bonded only by hydrogen bonds. They report an increase in wafer bond energy with aging at temperatures below 110 °C for long times, and attribute this to increased hydrogen bonding due to rearrangement of water molecules. We observe that a higher mobility of water molecules and silanols at the higher simulation temperature results in rearrangement and more hydrogen bridging across the interface.

Neutron diffraction,[47] magic angle spinning nuclear magnetic resonance,[48–50] and extended x-ray absorption fine structure[51] analyses have indicated that siloxane bond angles in bulk vitreous silica have a broad distribution between 100° and 180°, centered at approximately 145°–150°. Simulation data using the current potentials show good agreement with experiment.[34] Furthermore, simulations[21,23] indicate that reaction of water with the surface of vitreous silica removes bond angles below 130° via reaction with the strained siloxane bonds at these sites. Molecular orbital calculations[52,53] have shown that Si–O bonds are longer and less stable for members of low-angle siloxane bonds. Thus, the previous simulations indicate that the strained bonds associated with low angle siloxane bonds are unstable in the presence of water.

To gain further insight into the process of bond formation across the three interface types, mechanisms were determined by characterizing the species to which the three members of each siloxane bridge were bonded as the siloxane bridges formed and every 10 fs thereafter. The siloxane bond angles of bridges were also determined upon formation (and every 10 fs thereafter). Figure 4 shows bond angle distributions for siloxane bond angles that form across the pristine interfaces during the first 2.5 Å of the approach after siloxane bonding initiated. The stacked histogram in Fig. 4(a) shows the fraction of siloxane bridges that form across the interface between 1.75 Å interface separation and −0.75 Å separation [see Figs. 1(a) and 1(d)] with initial bond angles within ranges of 5° for the lower temperature pristine system. The siloxane bond angle data collected in this figure (and Figs. 5 and 6) are *instantaneous* bond angles determined as the bridges formed. The siloxane bridges are further categorized by the mechanism by which the bridges form. The bars are stacked to indicate the overall fraction of bond angles that lie within the range of interest. The contribution of each mechanism is indicated by the magnitude of each bar in the stack.

Figure 4(a) shows that the initial bridges across the lower temperature pristine interface formed primarily by two mechanisms, resulting in a bimodal distribution. At high bond angles (>155°), the majority of these bonds formed by an SN_2-type reaction. This reaction involves the temporary formation of a 5-coordinated Si atom (SiO_5) due to bonding between a nonbridging oxygen (NBO) on one surface and a 4-coordinated Si on the other. The coordination polyhedron around the Si atom of interest changes from a tetrahedron to a trigonal bipyramid. The remainder of the high-angle siloxane bridges form by bonding of an NBO to a 3-coordinated Si atom (SiO_3) (on opposite surfaces). Temporally, these high-angle bonds formed before the bridges with angles less than 135° in the figure. The pristine surfaces stretch out to each other to form these bonds. This is further supported by the observation that these bonds form under conditions of net attraction between the surfaces [Fig. 1(a)].

The mechanism of siloxane bridge formation for the lower bond angles in pristine silica was the formation of overcoordinated O atoms (O bonded to 3 Si, OSi_3) due to

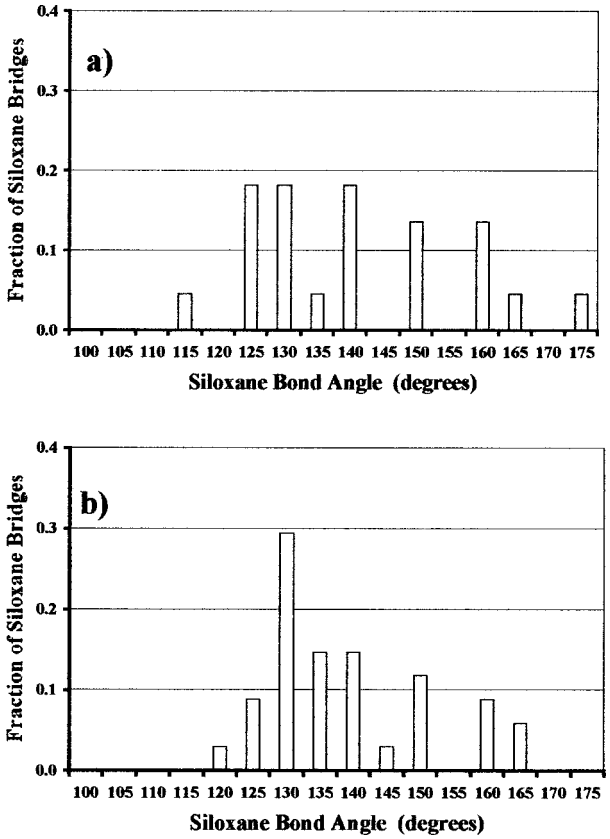

FIG. 5. The fraction of siloxane bridges that form across the hydroxylated interfaces with the initial siloxane bond angles within the indicated ranges at: (a) 300 K and (b) 1000 K. All bridges form by the SN_2 reaction. Data are from bonds that form after the surfaces move 2.5 Å closer than the distance of the first siloxane bond formation.

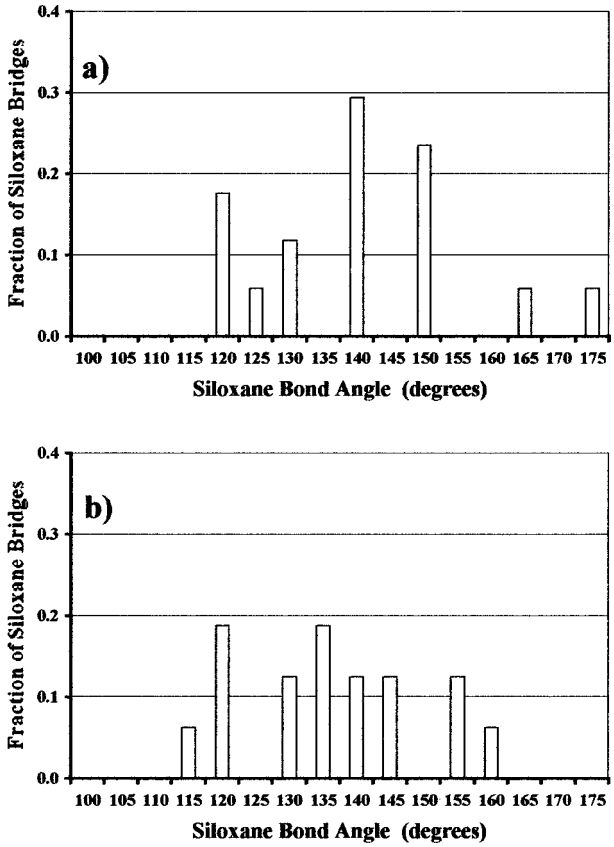

FIG. 6. The fraction of siloxane bridges that form across the wet interfaces with the initial siloxane bond angles within the indicated ranges at: (a) 300 K and (b) 1000 K. All bridges form by the SN_2 reaction. Data are from bonds that form after the surfaces move 2.5 Å closer than the distance of the first siloxane bond formation.

bonding between a two-coordinated oxygen on one surface and a silicon atom on the other. This silicon participating in the bond was very rarely observed to be 5 coordinated after formation of the new bond, indicating that this silicon was undercoordinated (SiO_3) prior to forming the new bond to the OSi_3 species. The low siloxane bond angles observed for these species are consistent with the trigonal geometry for OSi_3 species in silica.[54,55]

The change in mechanism from the SN_2 reaction to OSi_3 formation as the surfaces got closer to one another is consistent with the onset of contact between the silica networks of both surfaces. Since NBOs relax outward on a silica surface, one would expect mechanisms involving NBOs to dominate initial bond formation, as we observe. As the silica networks come in contact, our results indicate that OSi_3 mechanisms dominate bond formation. It should be noted that this change in mechanism does not correspond to elimination of NBO on the surfaces by bond formation. An average of 5.5 NBO/nm^2 were present on each surface, yet less than 1 bond/nm^2 was present across the interface when the OSi_3 mechanism began to dominate. Thus network contact occurs prior to elimination of surface NBO. This is due to surface roughness on the scale of several angstroms.

The initial bond angle data for bonds that form between approach distances of 1.75 and -0.75 Å in the higher temperature pristine interface are collected in Fig. 4(b). The results are very similar to those for the lower temperature system, indicating that in this temperature range the mechanisms of initial bridge formation are not dependent on temperature within this temperature range.

Figure 5 presents initial siloxane bond angle distributions for the hydroxylated systems over intervals of the approach similar to those of Fig. 4. Siloxane bonds that form between interface separations of -0.5 and -3 Å for the lower temperature system are characterized in Fig. 5(a). In contrast to the bimodal distribution in the pristine systems in Fig. 4, a broad distribution was observed. Only the SN_2-type reaction mechanism was observed, even for the low-angle bridges. Since SiO_3 were removed from the surfaces by reaction with water molecules during hydroxylation, no bridges were formed by NBO bonding to SiO_3. No OSi_3 were observed to form, either. Comparing Fig. 4(a) to Figs. 5(a) and 5(b), the majority of the bond angles below 145° in the pristine systems are also below 125°, whereas the majority of the bond angles below 145° in the hydroxylated systems are also above 125°. This suggests that the low bond angles required to form OSi_3 species in the pristine systems are not stable when hydrogen is present. Furthermore, due to hydroxylation of the surfaces by the reactions mentioned above, the O:Si ratio on hydroxylated surfaces was higher than on pristine surfaces. This would favor the formation of SiO_5 over that of OSi_3.

The bond angle data for the higher temperature hydroxylated system is presented in Fig. 5(b). Again, a broad distribution was observed. Comparing Fig. 5(b) to 5(a), the higher temperature distribution [Fig. 5(b)] was more skewed to lower angles.

The initial siloxane bond angle distributions for the wet systems are shown in Fig. 6. Figure 6(a) shows the data for the lower temperature wet system gathered between interface separations of -2.25 and -4.75 Å. A broad distribution of angles was observed, similar to the hydroxylated interface data in Fig. 5. Again, only the SN_2-type mechanism was observed. The higher temperature bond angle distributions in Fig. 6(b) were again similar to the lower temperature distributions, with a slight skewing to lower bond angles again apparent. Thus, the mechanism of siloxane bridge formation in wet systems is the same as in hydroxylated systems: the SN_2 reaction. The higher applied stress required to bond systems with water trapped at the interface [Fig. 1(c)] may be associated with the limited volume available to the trapped water.

As mentioned above, the bond angle data in Figs. 4, 5, and 6 were collected instantaneously as the siloxane bridges formed. This was done to characterize the mechanisms by which the bonds formed. As discussed previously, mean siloxane bond angles between 145° and 150° have been reported for bulk vitreous silica from experiments and simulations. A broad distribution about the mean was reported in these studies, indicating that bond angles range from 120° to near 180°. However, many of the bond angles in Figs. 4, 5, and 6 are in the high and low tails of distributions reported for bulk glass. Thus these bonds are strained as they form. To gain insight into the equilibrium bond angles of siloxane bridges across the interface, 50 ps simulations with no advancement of the top surface were run at the end of each of the 2.5 Å intervals discussed above for each system type. Instantaneous siloxane bond angles at the end of these runs were compared to the initial bond angles reported in Figs. 4, 5, and 6. The majority of these equilibrium bond angles were between 140° and 160° independent of the surface treatment, consistent with siloxane bond angles observed in bulk silica. No equilibrium bond angles below 130° were observed, although some bond angles above 160° remained, indicating that higher than average siloxane bond angles are more stable at these interfaces than lower than average bond angles. This is consistent with the *ab initio* calculations that showed that Si–O bonds at smaller siloxane bond angles are less stable than those bonds at larger bond angles.[52,53] Simulations similarly show longer Si–O bonds at smaller siloxane bond angles, implying less stable bonds.[22] In most cases, the changes in the bond angles to intermediate angles were due to relaxation of the overcoordinated defects (SiO_5 or OSi_3) that formed as the bridges formed across the interface. This indicates that these defects act as intermediates in the bonding of these interfaces.

IV. CONCLUSIONS

Pristine silica surfaces showed siloxane bond formation via coalescence of undercoordinated defects and formation of overcoordinated silicon defects (SiO_5) by an SN_2^- type reaction. The initial siloxane bridges form by extension of each surface, forming at bond angles that are larger than the bulk average (which is near 150°). With a slightly closer approach between the surfaces (2.5 Å closer, which brings the surfaces towards the bulk-like density), additional siloxane bonds across the interface form at angles much less than the bulk average. The lower set of bond angles in this bimodal distribution of siloxane bond angles would be more reactive with moisture than those near the bulk average.

Simulations of hydroxylated interfaces containing silanols but no excess water molecules initially exhibited only hydrogen bonding across the interface. Application of compressive stress resulted in the breakage of the H-bonded bridges and the formation of siloxane bridges exclusively by an SN_2 reaction. Higher temperature enhanced the formation of the siloxane bridges. The siloxane bridges form a more uniform distribution of siloxane bond angles from 115° to 180°, although they are skewed below 150°. However, the very low and reactive bond angles that were observed in the pristine system were not observed in the hydroxylated case.

Simulations of interfaces formed with water molecules between the surfaces also exhibited only hydrogen bonding initially. Again, such bonding was enhanced at the higher temperature. Since the water molecules were not allowed to escape from the system in these simulations, high compressive stress was required to obtain siloxane bond formation across the interface. Siloxane bridges formed by SN_2 reactions at bond angles similar to those observed in the hydroxylated systems. Water molecules entered into the subsurface of the silica along ''channels'' caused by the normal network structure of amorphous silica.

The presence of silanols or water molecules initially enhances hydrogen bonding between the surfaces, consistent with experiment. The rate of siloxane bond formation in the hydroxylated case is nearly the same as in the pristine case. However, too many water molecules trapped between the silica surfaces were found to inhibit initial siloxane bond formation in comparison to completely pristine silica surfaces. A compressive stress was required to initiate this bond formation in the presence of trapped moisture. In addition, the wet case with excess water present showed a bond formation rate that was slower than either the pristine or hydroxylated cases. Regions of real bonded wafers that have water molecules trapped between the wafers will experience less interfacial siloxane bonding unless either high temperatures are used to remove the water or compressive stresses are used. The former is the current method for removing water and attaining high bonding strengths of bonded wafers.

ACKNOWLEDGMENT

The authors would like to acknowledge support from the New Jersey Commission on Science and Technology.

[1] S. Bengtsson, J. Electron. Mater. **21**, 841 (1992).
[2] J. B. Lasky, S. R. Stiffler, F. R. White, and J. R. Abernathey, in *Silicon-on-Insulator (SOI) by Bonding and Etch-back* (IEEE, Washington DC, 1985), pp. 684–687.
[3] W. P. Maszara, J. Electrochem. Soc. **138**, 341 (1991).

[4] M. Shimbo, K. Furukawa, K. Fukuda, and K. Tanzawa, J. Appl. Phys. **60**, 2987 (1986).
[5] Q.-Y. Tong and U. Gosele, Mater. Chem. Phys. **37**, 101 (1994).
[6] Q.-Y. Tong and U. Gosele, *Semiconductor Wafer Bonding: Science and Technology* (Wiley, New York, 1998).
[7] Q.-Y. Tong and U. Gosele, J. Electrochem. Soc. **143**, 1773 (1996).
[8] W. P. Maszara, B.-L. Jiang, A. Yamada, G. A. Rozgonyi, H. Baumgart, and A. J. R. de Kock, J. Appl. Phys. **69**, 257 (1991).
[9] R. Stengl, K.-Y. Ahn, and U. Goesele, Jpn. J. Appl. Phys., Part 2 **27**, L2364 (1988).
[10] W. P. Maszara, G. Goetz, A. Caviglia, and J. B. McKitterick, J. Appl. Phys. **64**, 4943 (1988).
[11] M. Grundner, J. Vac. Sci. Technol. A **5**, 2011 (1987).
[12] M. K. Weldon, V. E. Marsico, Y. J. Chabal, D. R. Hamann, S. B. Christman, and E. E. Chaban, Surf. Sci. **368**, 163 (1996).
[13] G. Kissinger and W. Kissinger, Phys. Status Solidi **123**, 185 (1991).
[14] Q.-Y. Tong, T.-H. Lee, U. Gosele, M. Reiche, J. Ramm, and E. Beck, J. Electrochem. Soc. **144**, 384 (1997).
[15] Q.-Y. Tong, W. J. Kim, T. H. Lee, and U. Goesele, Electrochem. Solid-State Lett. **1**, 52 (1998).
[16] M. Horiuchi and S. Aoki, J. Electrochem. Soc. **139**, 2589 (1992).
[17] G. E. Maciel and D. W. Sindorf, J. Am. Chem. Soc. **102**, 7606 (1980).
[18] B. C. Bunker, D. M. Haaland, T. A. Michalske, and W. L. Smith, Surf. Sci. **222**, 95 (1989).
[19] C. J. Brinker, R. J. Kirkpatrick, D. R. Tallant, B. C. Bunker, and B. Montez, J. Non-Cryst. Solids **99**, 418 (1988).
[20] C. J. Brinker, R. K. Brow, D. R. Tallant, and R. J. Kirkpatrick, J. Non-Cryst. Solids **120**, 26 (1990).
[21] B. P. Feuston and S. H. Garofalini, J. Appl. Phys. **68**, 4830 (1990).
[22] S. H. Garofalini, J. Non-Cryst. Solids **120**, 1 (1990).
[23] E. B. Webb and S. H. Garofalini, J. Non-Cryst. Solids **226**, 47 (1998).
[24] T. A. Michalske and B. C. Bunker, J. Appl. Phys. **56**, 2686 (1984).
[25] T. A. Michalske and E. Fuller, J. Am. Ceram. Soc. **68**, 586 (1985).
[26] R. K. Iler, *The Chemistry of Silica* (Wiley, New York, 1979).
[27] S. H. Garofalini, in *Proceedings of the Second International Conference on Semiconductor Wafer Bonding*, edited by M. A. Schmidt, T. Abe, C. Hunt, and H. Baumgart (The Electrochemical Society, Pennington, NJ, 1993), Vol. 93-29, pp. 57–70.
[28] E. B. Webb and S. H. Garofalini, J. Chem. Phys. **101**, 10101 (1994).
[29] E. B. Webb and S. H. Garofalini, Surf. Sci. **319**, 381 (1994).
[30] S. H. Garofalini, E. B. Webb, and D. A. Litton, in *Semiconductor Wafer Bonding: Science, Technology, and Applications*, edited by U. Gosele, H. Baumgart, T. Abe, C. Hunt, and S. Iyer (The Electrochemical Society, Pennington, NJ, 1998), Vol. 99-36, pp. 37–45.
[31] D. Timpel, M. Schaible, and K. Scheerschmidt, J. Appl. Phys. **85**, 2627 (1999).
[32] B. F. Feuston and S. H. Garofalini, J. Phys. Chem. **94**, 5351 (1990).
[33] S. H. Garofalini and H. Melman, in *Application of Molecular Dynamics Simulations To Sol-Gel Processing*, Aneheim, 1986 (Materials Research Society, Pittsburgh, PA), pp. 497–505.
[34] B. P. Feuston and S. H. Garofalini, J. Chem. Phys. **89**, 5818 (1988).
[35] B. F. Feuston and S. H. Garofalini, J. Chem. Phys. **91**, 564 (1989).
[36] S. H. Garofalini and G. Martin, J. Phys. Chem. **98**, 1311 (1994).
[37] G. Martin and S. H. Garofalini, J. Non-Cryst. Solids **171**, 68 (1994).
[38] S. Blonski and S. H. Garofalini, Surf. Sci. **295**, 263 (1993).
[39] W. C. Mackrodt, R. J. Davey, S. N. Black, and R. Docherty, J. Cryst. Growth **80**, 441 (1987).
[40] I. G. Batirev, A. Alavi, M. W. Finnis, and T. Deutsch, Phys. Rev. Lett. **82**, 1510 (1999).
[41] M. Garcia, E. Webb, and S. H. Garofalini, J. Electrochem. Soc. **145**, 2155 (1998).
[42] S. H. Garofalini, J. Chem. Phys. **78**, 2069 (1983).
[43] M. I. Trioni, A. Bongiorno, and L. Colombo, J. Non-Cryst. Solids **220**, 164 (1997).
[44] C. P. Pantano, J. F. Kelso, and M. J. Suscavage, in *Advances in Materials Characterization*, edited by D. R. Rossington, R. A. Condrate, and R. L. Snyder (Plenum, New York, 1983), Vol. 15, pp. 1–38.
[45] S. M. Levine and S. H. Garofalini, J. Chem. Phys. **88**, 1242 (1988).
[46] A. E. Kohler and S. H. Garofalini, Langmuir **10**, 4664 (1994).
[47] A. C. Wright, A. G. Clare, and D. I. Grimley, J. Non-Cryst. Solids **112**, 33 (1989).
[48] E. Dupree and R. F. Pettifer, Lett. Nature **308**, 523 (1984).
[49] L. Gladden, T. Carpenter, and S. Elliott, Philos. Mag. B **53**, L81 (1986).
[50] R. F. Pettifer, R. Dupree, I. Farnan, and U. Sternberg, J. Non-Cryst. Solids **106**, 408 (1988).
[51] G. N. Greaves, A. Fontaine, P. Lagarde, D. Raoux, and S. J. Gurman, Nature (London) **293**, 611 (1981).
[52] M. D. Newton and G. V. Gibbs, Phys. Chem. Miner. **6**, 221 (1980).
[53] G. V. Gibbs, Am. Mineral. **67**, 421 (1982).
[54] G. Lucovsky, Philos. Mag. B **39**, 513 (1979).
[55] S. H. Garofalini, J. Non-Cryst. Solids **63**, 337 (1984).